Short communication

Performance of a novel La(Sr)MnO$_3$-Pd composite current collector for solid oxide fuel cell cathode

Chuan Wang [a], Xianshuang Xin [a], Yanjie Xu [a], Xiaofeng Ye [a], Lijun Yu [b], Shaorong Wang [a,*], Tinglian Wen [a]

[a] CAS Key Laboratory of Materials for Energy Conversion, Shanghai Institute of Ceramics, Chinese Academy of Sciences (SICCAS), 1295 Dingxi Road, Shanghai 200050, PR China
[b] Energy Research Institute, Shanghai Jiaotong University, Shanghai 200030, PR China

ABSTRACT

The electrochemical performance of LSM–Pd composite material as current collector of SOFC cathode is studied on $(La_{0.8}Sr_{0.2})_{0.9}MnO_3$ (LSM90) cathode. The influence of Pd content on contact resistance is investigated. The investigation shows that the contact resistance of LSM–Pd is about $20\,m\Omega\,cm^2$ at 750 °C when the composite contains 8 wt% Pd, and it could be comparable to pure Pt. The ohmic resistance of a single cell using LSM–Pd composite is about $255\,m\Omega\,cm^2$ that contains 4 wt% Pd as current collector, this value is close to that of a cell using expensive Pt paste as current collector.

© 2011 Elsevier B.V. All rights reserved.

1. Introduction

Solid oxide fuel cell (SOFC) has received so much attention in last two decades because of its promise of higher efficiency and lower pollutant emission in comparison to other conventional energy conversion devices such as internal combustion engine and turbines [1,2]. Furthermore, it has good fuel flexibility that allows a variety of fuels (including those derived from renewable sources) to be employed.

Lanthanum strontium manganite (LSM), yttria-stabilized zirconia (YSZ) and Ni–YSZ are the most conventional cathode, electrolyte, and anode materials, respectively [1,3] for high temperature SOFC. To obtain a higher power density at intermediate temperature, it is necessary to reduce the ohmic and polarization resistances. Polarization resistance can be reduced by using materials with high electrochemical reaction activity as cathode and anode, and by optimizing the microstructure at the electrode/electrolyte interface region. For example, a mixed conductor such as $(La,Sr)(Co,Fe)O_3$ can significantly reduce the polarization resistance [4,5]. On the other hand, the ohmic resistance of a single cell is usually reduced by making thinner the electrolyte film or adopting materials with higher conductivity (for example Scandia-stabilized zirconia, SSZ). For a SOFC stack, there are many single cells that are connected in series through interconnect materials. Therefore, the stack performance is decided by both the single cell and the contact between the electrode and the interconnector on both anode and cathode sides. In SOFC stacks, the contact resistance between the electrode and the interconnector then plays a very important role. To reduce the contact resistance, one current collector layer is added between an electrode and the interconnector. Contact resistance loss on the anode side is relatively small, where nickel metal is utilized to provide a low-resistance metallurgical bond between the anode and a metallic interconnect. It is more challenging to achieve low contact resistance on the cathode side, where at least one ceramic–metal interface and possibly several ceramic–ceramic interfaces exist. To achieve this aim, pure noble metals or ceramic materials have been attempted [6–12]. The prices of pure noble metals are too high, and this will add the cost of the whole cell stack. Meanwhile, the interface between ceramic cathode and metal current collector may have the mismatch of thermal expansion coefficient (TEC) between the current collector layer and cathode. Therefore, the long-term stability of a SOFC stack may be influenced. On the other hand, a ceramic current collector is not as flexible as metal, resulting in larger contact resistance. Further more the conductivity of a ceramic current collector is normally not high enough.

Therefore, considering the cost and stability of the stack, neither a pure metal nor a single phase ceramic could meet our requirement perfectly. Boulfrad et al. [13], recently reported that palladium (Pd)–$(La_{0.75}Sr_{0.25})_{0.97}Cr_{0.5}Mn_{0.5}O_3$ (LSCM) composite current collector for SOFC anode showed well adhesion between the current collection layer and the electrode. In the present work, fine Pd particle was used to connect the LSM particles, so that it had high enough electrical conductivity for being used as a current collector on the cathode side.

2. Experimental procedure

2.1. Synthesis of LSM particles

$La_{0.8}Sr_{0.2}MnO_3$ (LSM20) powder was synthesized using the conventional solid state reaction method. Obtained powder was pressed into rectangular bulks of 150 mm × 150 mm × 10 mm under a pressure of 100 MPa. The bulks were fired at 1350 °C for 5 h, and then broken to small particles and sieved. The particle size was measured by a laser particle analyzer (Malvern, Mastersizer2000).

2.2. Electrical conductivity ant TEC measurements

Pd was gained from Tetraamminepalladium(II) chloride ($Pd(NH_3)_4Cl_2$) that was dissolved readily in water and was decomposed at about 120 °C in the present work. The actual Pd content was analyzed by heating them to complete decomposition at 500 °C. The LSM20 particles and $Pd(NH_3)_4Cl_2$ solution were mixed in the following proportions: $(100 − x)$wt%LSM20 + $x$wt%Pd, where x = 0, 1, 1.5, 2.5, 4, 6 and 8, and named from LSM–Pd0 to LSM–Pd6 in proper order. The composites of LSM–Pd were heat treated at 450 °C for 2 h. For electrical conductivity and TEC studies, cylindrical specimens of the composites were prepared by uniaxial pressing at a pressure of 100 MPa. The length and diameter of the specimens are 15–20 and 5 mm, respectively. The sintering temperature of samples was adopted at 900 °C in present work, in order to make the data valuable for stack preparation, where green current collecting layer will be used and sintered at the sealing temperature of 900 °C. The cylindrical specimens were heated to 900 °C at 3 °C min^{-1} in air and held at this temperature for 2 h. TEC measurements were conducted using a NETZSCH DIL 402C dilatometer in air using a heating rate of 5 °C min^{-1}. After that, electrical conductivity measurements were conducted via the four-probe DC method.

2.3. Contact resistance measurements

A-site deficient LSM was reported to exhibit enhanced sintering ability and stability in air and nitrogen compared to ordinary LSM [14]. $(La_{0.8}Sr_{0.2})_{0.9}MnO_3$ (LSM90) powder was synthesized by solid state reaction method. The obtained LSM90 powder was used for preparing a LSM90 film of ∼150 μm thickness with tape casting method. The LSM–Pd composite, as current collector, was screen printed onto the both sides of the sintered LSM90 film (relative density 95%). Then Ag mesh was contacted to the surface of LSM–Pd current collector, on both sides, to measure the contact resistance. The measurement was carried out from 850 °C to 600 °C in air,

by 4 probe complex impedance method, using an electrochemical workstation IM6e (Zahner, GmbH, Germany). To evaluate the experimental result, Pt paste was also brushed onto the LSM film and tested as a reference. For the blank sample there is no current collector at all on the LSM film.

2.4. Single cell test

Single cell preparation and test setup were basically similar to that proposed by Ye et al. [15,16], and is illustrated in Fig. 1. Ni/YSZ was used as anode support layer (1 mm), commercial $Zr_{0.89}Sc_{0.1}Ce_{0.01}O_{2−x}$ (SSZ, Daiichi Kigenso Kagaku Kogyo, Japan) for electrolyte layer (8–10 μm), and the $La_{0.8}Sr_{0.2}MnO_{3−x}$ (LSM, 5.78 m^2 g^{-1}, fuel cell materials.com)–SSZ (LSM–SSZ) (70% LSM and 30% SSZ by mass) composite was used for cathode layer (15–20 μm). Au lead wires were attached to the surface of the anode and cathode. The cathode side of the setup was then attached to the alumina tube and the edge was sealed using a glass ring. The setup must be kept in 850 °C for 1 h before the cell test so that the glass could be soften sufficiently. LSM–Pd was used as the current collector in cathode by screen-printing. To on the other side, nickel felt was chosen as the current collector on anode. Two Au lead wires were attached to the surface of the both current collection layers. The current–voltage curves and electrochemical impedance spectroscopy were obtained by IM6e.

3. Results and discussion

3.1. Distribution of LSM20 particle

Fig. 2 shows the distribution of LSM20 particles. The average size of LSM20 particles was about 3 μm, and the particles were distributed in a narrow space so that 80% particles were among 2 μm and 4 μm. The narrow particle distribution could ensure sufficient porosity because there were few small particles to fill the blank between big particles. So that oxygen could permeate well through when the stack was working.

3.2. Electrical conductivity and TEC dependence on Pd content

The thermal expansion coefficients of the specimens are shown in Table 1. The TEC values for LSM–Pd between 30 °C and 900 °C range from $13.08 × 10^{-6}$ K^{-1} to $12.42 × 10^{-6}$ K^{-1}, decreasing with Pd content. Several models have been developed aiming to quantitatively explain the dependence of TEC on particle volume fraction. The simplest approach is the linear rule of mixtures (ROM), $\alpha_c = V_p\alpha_p + (1 − V_p)\alpha_m$.
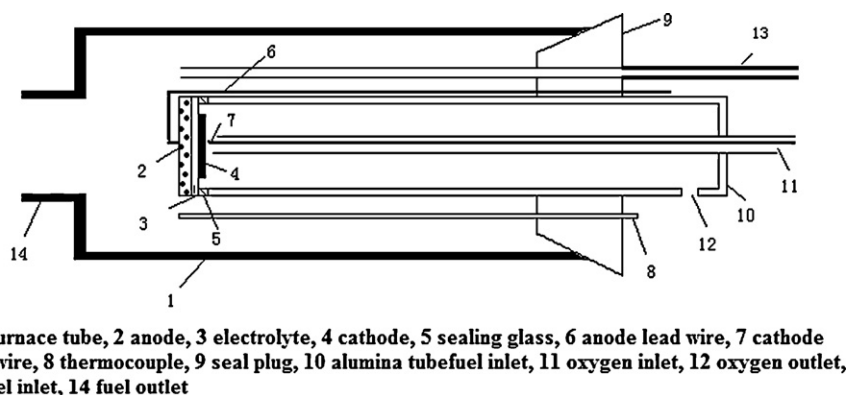

1 furnace tube, 2 anode, 3 electrolyte, 4 cathode, 5 sealing glass, 6 anode lead wire, 7 cathode lead wire, 8 thermocouple, 9 seal plug, 10 alumina tubefuel inlet, 11 oxygen inlet, 12 oxygen outlet, 13 fuel inlet, 14 fuel outlet

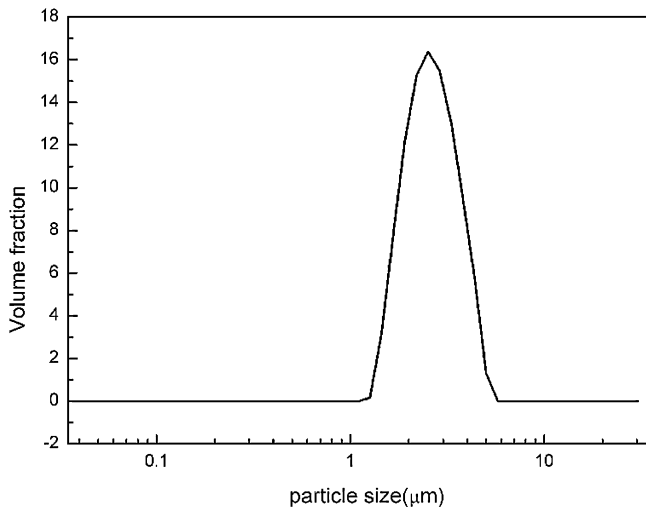**Fig. 1.** Schematic drawing of single cell test setup.

Fig. 2. The distribution of LSM particles.

Table 1
TEC of the LSM–Pd composite as function of Pd mass fraction.

	LSM–Pd0	LSM–Pd1	LSM–Pd2	LSM–Pd3	LSM–Pd4	LSM–Pd5	LSM–Pd6
TEC (10^{-6} K^{-1})	13.08	12.86	12.64	12.57	12.50	12.46	12.42

Hereafter we shall refer to the thermal expansion coefficient by means of either TEC or α, and the subscripts m and p denote metal and LSM20 particle, respectively. The TEC of pure Pd is smaller than 12×10^{-6} K^{-1}. Therefore, the TEC of LSM–Pd composite decreases with increasing Pd content.

Fig. 3 shows the electrical conductivity (σ) plots versus temperature. There are porous in the samples for the samples are not sintered in high temperate. Therefore, the conductivity of the sample is not so high compared to a dense sintered compact. The σ does not increase a lot when the Pd content is less than 4 wt% for there is not enough Pd to connect the LSM particle. The σ has a sharp increase when the Pd content is more than 4 wt%, which is almost twice as LSM–Pd3. The Pd content is so small, and the Pd particles are used just to connect LSM particles. The conductivity does
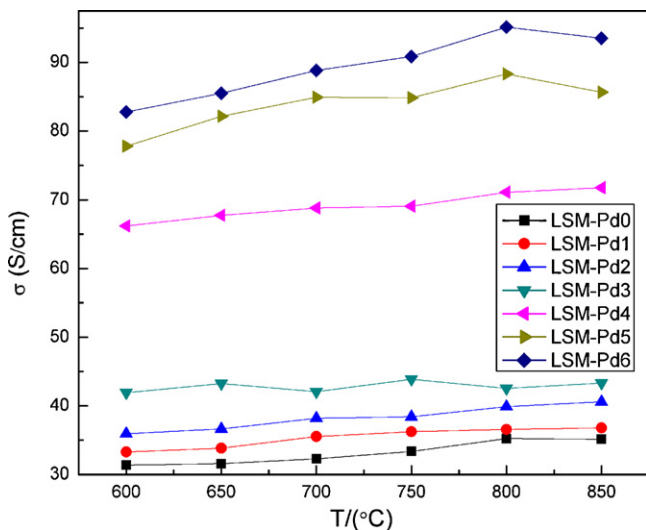
not change greatly with the measuring temperature, this maybe because of the fact that it consists of contributions from both Pd metal and LSM ceramic conducting phases.

The electron microscope images of the LSM–Pd composite after electrical conductivity measurement are shown in Fig. 4. For the sample without Pd (LSM–Pd0), the adhesion behavior between LSM particles is poor, therefore, the conductivity is low. For other samples, Pd particles distribute uniformly on LSM particles, and play a role of connecting the LSM particles. The electrical conductivity is not high enough for there is not enough Pd in LSM–Pd1, LSM–Pd2 and LSM–Pd3 samples to connect LSM particles. Then the quality of contact between LSM particles is improved by using larger amount of Pd in the composite. There are obvious Pd particle could be seen from LSM–Pd4, resulting in a sharp increase in conductivity. Fig. 4f is high magnification of LSM–Pd4, and it can be seen clearly there are small Pd particles between LSM particles and Pd particles play part in connecting LSM particles.

3.3. Contact resistance dependence on Pd content

Fig. 5 shows the relationship of contact resistance versus temperature. Adding a current collecting layer onto the LSM film could decrease the contact resistance obviously. The contact resistance was further decreased with the increase of Pd content, which is coincidence with the result of conductivity experiment. The contact resistance of LSM–Pd6 is about 20.12 mΩ cm^2 that is comparable to that of Pt paste. This result shows that an unsintered LSM–Pd6 current collecting layer, with its flexibility and improved conductivity, may have the potential to improve the contact between an LSM cathode and alloy interconnector.

3.4. Single cell performance

To evaluate the properties of the obtained LSM–Pd composite current collector further, a single cell was prepared by screen-printing LSM–Pd4 paste onto cathode. Pt paste was chosen as reference again. Fig. 6 shows the current density–voltage (I–V) and current density power density (I–P) curves measured at 750 °C. The open circuit voltage (OCV) values are all above 1.10 V, which is in good agreement with the theoretical value calculated from the Nernst equation. Fig. 7 shows the impedance spectroscopy measured under open circuit condition at 750 °C. The high frequency intercept with the X axis represents the ohmic resistance of the cell (R_o), involving the resistance of the electrolyte, electrodes and current collector, and the contact resistance associated with interfaces (contribution from lead wires was not involved due to the 4 probe method). The ohmic resistance of the cell using LSM–Pd4 as current collector is about 255 mΩ cm^2, which is close to that of a cell using Pt paste as current collector (190 mΩ cm^2). On the other hand, the polarization resistance (R_P) of the cell using LSM–Pd4 as current collector is almost three times as the cell using Pt paste as current collector and this leads to the sharp drop of cell using LSM–Pd4 current collector. The reason may be that when Pt paste is used as current collector, it may have an effect to improve the cathode reaction activity [17]. Another reason may be the gas diffusion polarization of the LSM–Pd4 layer. To verify the conjecture, LSM–Pd4 added with 10 wt% carbon black (LSM–Pd4–10C) is printed on the same cell to be the current collector, the ohmic resistance is almost the same as the former LSM–Pd4 cell (262 mΩ cm^2), but the polarization resistance drops from 6 Ω cm^2 to 1.8 Ω cm^2. At the same time, the power density is almost 90% of the cell using Pt paste as current collector.

Fig. 3. Conductivity of the LSM–Pd composite as function of Pd mass fraction.
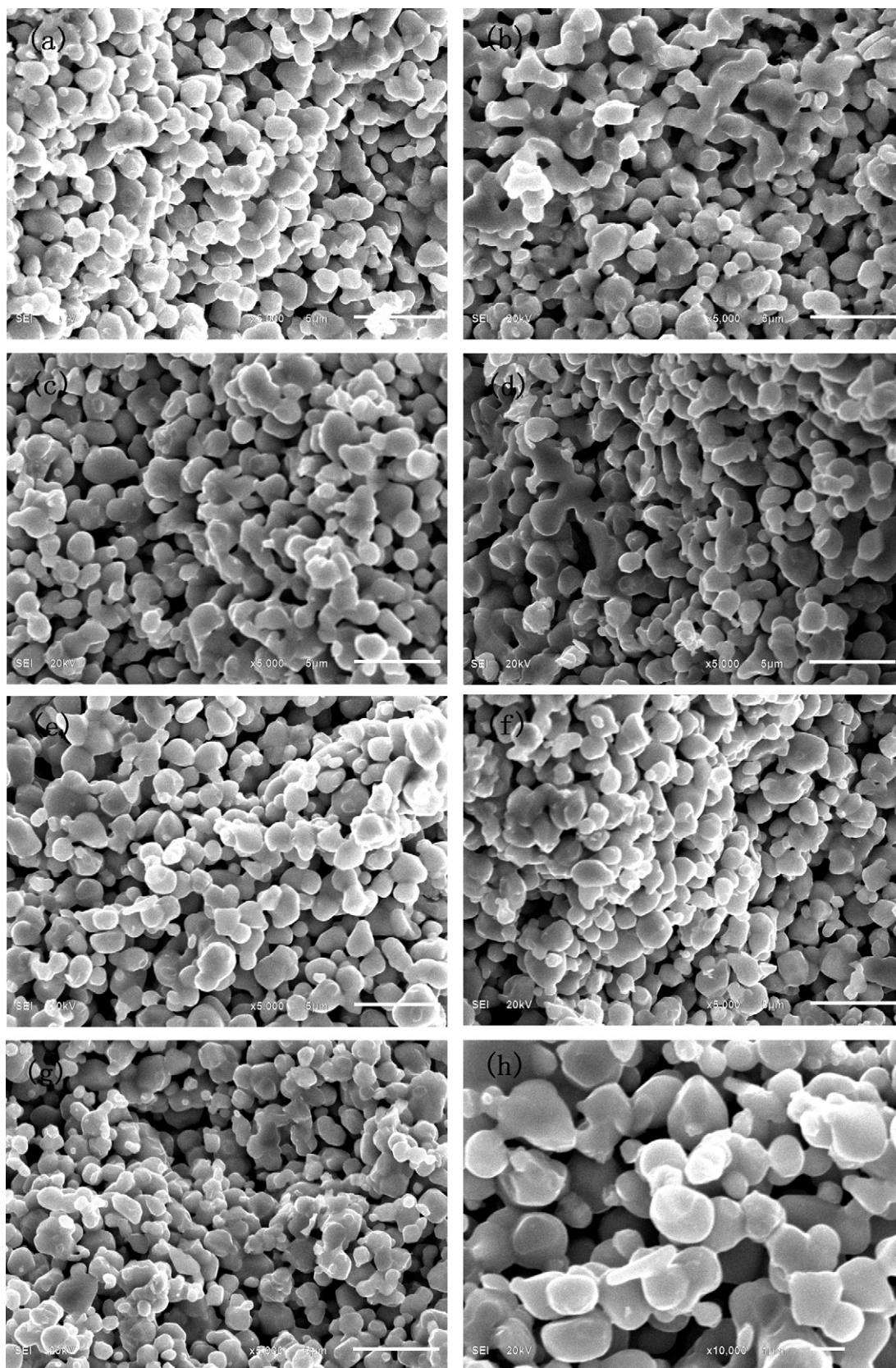
Fig. 4. SEM images of LSM–Pd composite. (a) LSM–Pd0, (b) LSM–Pd1, (c) LSM–Pd2, (d) LSM–Pd3, (e) LSM–Pd4, (f) LSM–Pd5, (g) LSM–Pd6, (f) high magnification of LSM–Pd4.
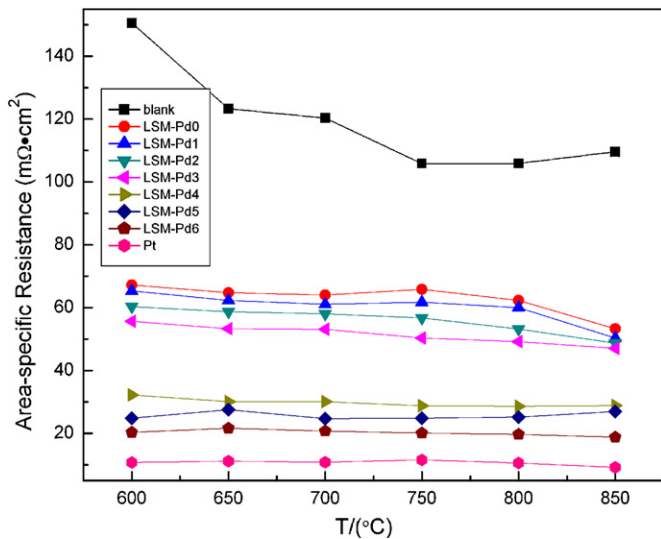
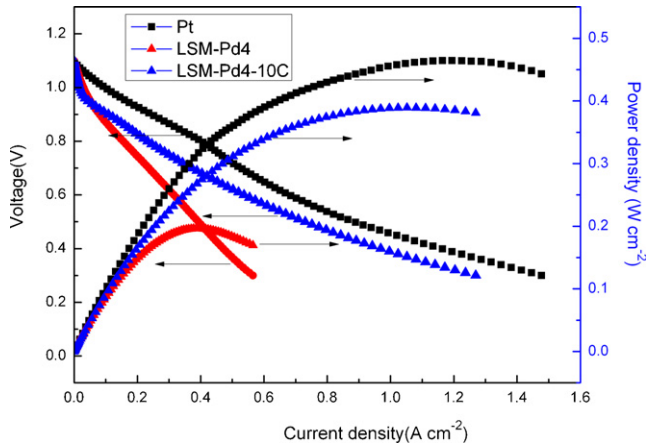**Fig. 5.** Contact resistance between LSM–Pd current layer and the cathode.

Fig. 6. I–V and I–P curves of the single cells measured at 750 °C.
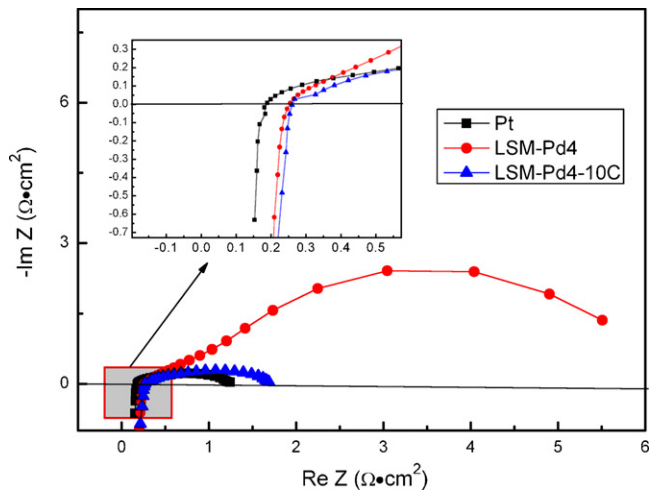

Fig. 7. Impedance spectrums of the single cells measured in the open circuit state at 750 °C.

4. Conclusion

The TEC and electrical conductivity were investigated for Pd–LSM composites as a function of the mass fraction of Pd. The TEC of the composites decreases with the increase of Pd content. When containing Pd 8 wt%, the TEC of the composite is $12.42 \times 10^{-6}\,K^{-1}$ which is almost the same as LSM20 cathode [18]. The Pd particles could connect LSM particles well when the Pd content is above 4 wt%. Single cell test also shows that LSM–Pd composite is a promising current collector material, especially adding 10 wt% carbon black in LSM–Pd, the power density is almost 90% of the cell using Pt paste as current collector.

Acknowledgements

References

[1] R.M. Ormerod, Chemical Society Reviews 32 (2003) 17–28.
[2] A. Atkinson, S. Barnett, R.J. Gorte, J.T.S. Irvine, A.J. McEvoy, M. Mogensen, S.C. Singhal, J. Vohs, Nature Materials 3 (2004) 17–27.
[3] N.P. Brandon, S. Skinner, B.C.H. Steele, Annual Review of Materials Research 33 (2003) 183–213.
[4] F. Tietz, V.A.C. Haanappel, A. Mai, J. Mertens, D. Stover, Journal of Power Sources 156 (2006) 20–22.
[5] F.S. Baumann, J. Fleig, H.U. Habermeier, J. Maier, Solid State Ionics 177 (2006) 1071–1081.
[6] M. Mori, Y. Liu, T. Itoh, Journal of the Electrochemical Society 156 (2009) B1182–B1187.
[7] S.P. Simner, M.D. Anderson, L.R. Pederson, J.W. Stevenson, Journal of the Electrochemical Society 152 (2005) A1851–A1859.
[8] H. Zhong, H. Matsumoto, T. Ishihara, A. Toriyama, Journal of Power Sources 186 (2009) 238–243.
[9] M. Mori, N.M. Sammes, E. Suda, Y. Takeda, Solid State Ionics 164 (2003) 1–15.
[10] J.W. Wu, C.D. Johnson, R.S. Gemmen, X.B. Liu, Journal of Power Sources 189 (2009) 1106–1113.
[11] J.H. Kim, R.H. Song, D.Y. Chung, S.H. Hyun, D.R. Shin, Journal of Power Sources 188 (2009) 447–452.
[12] J.H. Kim, R.H. Song, S.H. Hyun, Solid State Ionics 174 (2004) 185–191.
[13] S. Boulfrad, M. Cassidy, J.T.S. Irvine, Advanced Functional Materials 20 (2010) 861–866.
[14] B.P. McCarthy, L.R. Pederson, Y. Chou, X.D. Zhou, W.A. Surdoval, L.C. Wilson, Journal of Power Sources 180 (2008) 294–300.
[15] R. Zheng, X.M. Zhou, S.R. Wang, T.L. Wen, C.X. Ding, Journal of Power Sources 140 (2005) 217–225.
[16] X.F. Ye, B. Huang, S.R. Wang, Z.R. Wang, L. Xiong, T.L. Wen, Journal of Power Sources 164 (2007) 203–209.
[17] D.E. Vladikova, Z.B. Stoynov, A. Barbucci, M. Viviani, P. Carpanese, J.A. Kilner, S.J. Skinner, R. Rudkin, Electrochimica Acta 53 (2008) 7491–7499.
[18] G. Corbel, S. Mestiri, P. Lacorre, Solid State Sciences 7 (2005) 1216–1224.